

Distribution of grey matter atrophy in Huntington's disease patients: A combined ROI-based and voxel-based morphometric study

G. Douaud,^{a,*} V. Gaura,^a M.-J. Ribeiro,^b F. Lethimonnier,^{b,c} R. Maroy,^b C. Verny,^d P. Krystkowiak,^e P. Damier,^f A.-C. Bachoud-Levi,^{g,h} P. Hantraye,^{a,c} and P. Remy^{a,h}

^aURA CNRS-CEA 2210, Service Hospitalier Frédéric Joliot, 4, place du Général Leclerc, 91 401 Orsay, France

^bSHFJ, Orsay, France

^cIFR49, Orsay, France

^dDépartement de Neurologie, CHU Angers, France

^eCHRU Roger Salengro, Lille, France

^fClinique Neurologique-Centre d'Investigation Clinique-INSERM UMR 643, CHU Nantes, France

^gEquipe avenir INSERM U421, CHU Henri Mondor, Créteil, France

^hDépartement de Neurosciences, AP-HP, CHU Henri Mondor et Université Paris XII, Créteil, France

Received 25 November 2005; revised 29 March 2006; accepted 23 May 2006

Available online 27 July 2006

The striatum, a subcortical structure, is the principal target of the neurodegenerative process in Huntington's disease (HD). The measurement of striatal atrophy using the bicaudate ratio on CT scanner images has therefore been used for years to assess disease progression, but this measure only takes into account unidimensional changes in the head of the caudate nucleus. Recently, voxel-based morphometry (VBM), which permits automated statistical comparisons of whole-brain MRI images, has been proposed to quantify striatal atrophy. However, VBM was not originally designed to study subcortical structures, and severe deep brain deformations that occur in HD may hamper the automatic processing of VBM. Here, we validate the use of the optimised protocol of VBM to quantify subcortical atrophy in HD by comparing results obtained with this method to those provided by manual segmentation of subcortical structures. We studied 20 patients with early HD and 12 controls matched for age, sex and handedness using an improved T1-weighted sequence that eased grey matter segmentation. Both manual and automated methods evidenced the dorso-ventral gradient of striatal atrophy, a loss of grey matter in the globus pallidus and the thalamus, and similar correlations between clinical scores and subcortical atrophy. Furthermore, we were able to detect with VBM grey matter loss in the substantia nigra, the hypothalamus, the amygdala, the insular cortex and the premotor and sensorimotor cortices. Finally, VBM provided results consistent with previous post mortem results and proved to be a sensitive biomarker capable of correctly managing subcortical distortions throughout HD patients' brains.

© 2006 Elsevier Inc. All rights reserved.

Keywords: Huntington; Striatum; Atrophy; VBM; ROI; Neurodegenerative; Volumetry; Morphometry; Segmentation

Introduction

Huntington's disease (HD) is a lethal autosomic dominant degenerative disease resulting from an expansion of a CAG repeat within the IT15 gene on chromosome 4. The striatum is known to be the principal affected structure in HD patients. Indeed, the post mortem analysis of brain serial sections, providing the first measurements of neuropathological changes in Huntington's disease, demonstrated marked atrophy of the striatum (de la Monte et al., 1988; Lange et al., 1976). Besides, Vonsattel et al. (1985) showed that this striatal atrophy displayed a dorso-ventral gradient, and established a 5-point grading scale that has become the gold standard for neuropathological classification of HD. In this study, they found no discernible gross or microscopic neuropathological abnormalities in several cases of clinically diagnosed Huntington's disease. These cases were therefore labeled as 'grade 0'. Nevertheless, a recent whole-brain magnetic resonance imaging study has shown significant grey matter loss in the striatum of asymptomatic gene-positive subjects (Thieben et al., 2002). This suggests that striatal atrophy is an early marker of the neurodegenerative process in subjects carrying the HD mutation. Furthermore, it confirms that the measurement of striatal atrophy is relevant to monitor disease progression and therefore to identify the potential action of new treatments aiming to slow disease progression (Bloch et al., 2004) or to replace degenerated neurones (Bachoud-Lévi et al., 2000). The bicaudate ratio is the technique most commonly used to assess striatal atrophy in HD patients' in vivo images. This ratio is defined as the distance between the heads of the caudate nuclei at their narrowest separation as a percentage of the width of the brain along the same line. This method is, however, not satisfactory as it only takes into account unidimensional changes in a single structure of the striatum, the head of caudate. Moreover, although the striatum is

* Corresponding author. Fax: +44 1865 222729.

E-mail address: douaud@fmrib.ox.ac.uk (G. Douaud).

Available online on ScienceDirect (www.sciencedirect.com).

the main target of the neurodegenerative process, the mutation is distributed ubiquitously and several studies have reported the occurrence of atrophy in other subcortical and cortical regions in carriers of the HD mutation, either symptomatic or not (Kassubek et al., 2004; Rosas et al., 2003; Thieben et al., 2002). The quantification of atrophy in Huntington's disease subjects should therefore make use of imaging tools assessing whole-brain changes in three dimensions.

Voxel-based morphometry (VBM) permits an automated voxel-wise whole-brain statistical comparison of MRI scans using the statistical parametric mapping (SPM) software (Wellcome Department of Cognitive Neurology, London) (Ashburner and Friston, 2000). As such, VBM could afford clinicians of HD a unique biomarker, unbiased, reproducible and sensitive to infra-clinical manifestations (Thieben et al., 2002), which could both assess disease progression from an asymptomatic stage and refine inclusion criteria for experimental treatment protocols. However, VBM was not originally designed for the analysis of subcortical structures. In addition, even at an early stage of the disease, the deep brain regions already show severe deformations that may hamper the automatic processing of VBM analysis.

The aim of this work is therefore to validate the use of VBM for the quantification of subcortical atrophy in early HD patients, by comparison with regions of interest (ROI)-based morphometric measurements. More precisely, we investigated whether these two techniques provided similar results and whether they reproduced the data obtained in previous post mortem studies.

Methods

This study was part of the MIG-HD (Multicentric Intracerebral Grafting in Huntington's Disease) project and was approved by the ethics committee of Henri Mondor Hospital in Créteil. All subjects gave written informed consent.

Subjects

Twenty HD patients, twelve men and eight women, two of whom were left-handed, aged 26 to 57 years (44 ± 8 years), were included from four different hospitals (Nantes, Angers, Lille and Créteil). To meet inclusion criteria, all had genetically proven Huntington's disease with an abnormal number of CAG repeats, ranging from 40 to 57. They all had clinical symptoms for at least 1 year and 14 were at stage I of the disease according to their total functional capacity score ($TFC \geq 11$; Shoulson and Fahn, 1979), i.e., they were autonomous and could function fully both at work and at home. None has been grafted at the time of this study. We also selected 12 controls matched for age (41 ± 9 years), sex (7 M/5 F) and handedness (10 R/2 L) to the patients.

Each HD patient was examined using the Unified Huntington's Disease Rating Scale (UHDRS) (1996) in each hospital and the scores for each subscale (motor, behavioural, functional and neuropsychological) were collected. Additional motor tests including the Purdue Pegboard[®] and a hand-arm test (Langston et al., 1992) were performed.

Image analysis

Background and strategy

Our main objective was to quantify morphological changes in the deep brain grey nuclei of HD patients. The VBM method,

implemented within SPM software, has been recently used to assess brain morphometry in healthy or ill subjects but was not originally designed for the investigation of changes in subcortical structures, that show marked deformations in HD patients.

We therefore compared the automated VBM results with those obtained by a manual approach to validate the use of VBM for the morphological analysis of deep brain nuclei in patients with subcortical atrophy. We also evaluated and improved each step of the manual and automated methods, to make it possible to define, a posteriori, a strategy dedicated to subcortical morphometry in Huntington's disease patients. A schematic diagram of these steps is shown in Fig. 1.

1 Image acquisition. In a pilot study, whole-brain anatomical MRI was performed in five controls and five patients with mild Huntington's disease (not included in the present study) to assess the quality of the contrast between grey and white matter in the images. Images were initially acquired with a 1.5 T Signa imager (General Electric Healthcare, Milwaukee, WI) with a standard 3D T1-weighted inversion recovery fast spoiled gradient recalled (IR-FSPGR) sequence with the following parameters: axial orientation, matrix 256×256 , 124 slice locations, 0.9375×0.9375 mm² in-plane resolution, slice thickness 1.2 mm, TI/TE/TR (inversion/echo/repetition time) 600/2/10.2 ms, flip angle (α) 10°, read bandwidth (RBW) 12.5 kHz.

However, this acquisition provided images with an unsatisfactory contrast, particularly for the subcortical grey nuclei (Fig. 2). This lack of contrast is related to the higher transverse relaxation time found at 1.5 T in these structures than in the cortex (Steen et al., 1995), making subcortical grey matter difficult to distinguish from white matter. Therefore, as described below, we improved this T1-weighted sequence to enhance the contrast between grey and white matter.

2 Image contrast improvement. In all 12 controls and 20 HD patients studied here, MR images were acquired in the axial plane, with the same resolution ($0.9375 \times 0.9375 \times 1.2$ mm³), but using new parameters: TI/TE/TR = 620/2/20.3 ms, $\alpha = 10^\circ$, RBW = 7.81 kHz. Images obtained with this sequence can be compared with those provided by the standard sequence described in the previous paragraph in Fig. 2.

3 Manual segmentation. A single examiner (GD) delineated manually the striatal, pallidal and thalamic regions on each axial plane of each individual MRI scan, using Anatomist software (personal communication: Riviere et al., 2000). Improvement of the T1-weighted sequence facilitated discrimination of the outlines of these structures (Fig. 2).

All scans were reoriented and resampled so that the anterior and posterior commissures were located in the same axial plane, helping the reliable and reproducible identification of the structures. The various regions of interest (ROIs) in the striatum were defined as follows: the head and body of caudate nucleus were separated by axial projection of the most dorsal part of the putamen. The limit between the anterior and the posterior putamen was identified by axial projection of the anterior commissure (Morrish et al., 1996). We defined the ventral striatum as the ventral parts of the putamen and the head of the caudate when it was not possible to differentiate between these nuclei in the axial plane. The lowest limits of the globus pallidus and thalamus were defined on the AC-PC axial plane. Then, the accuracy of ROI

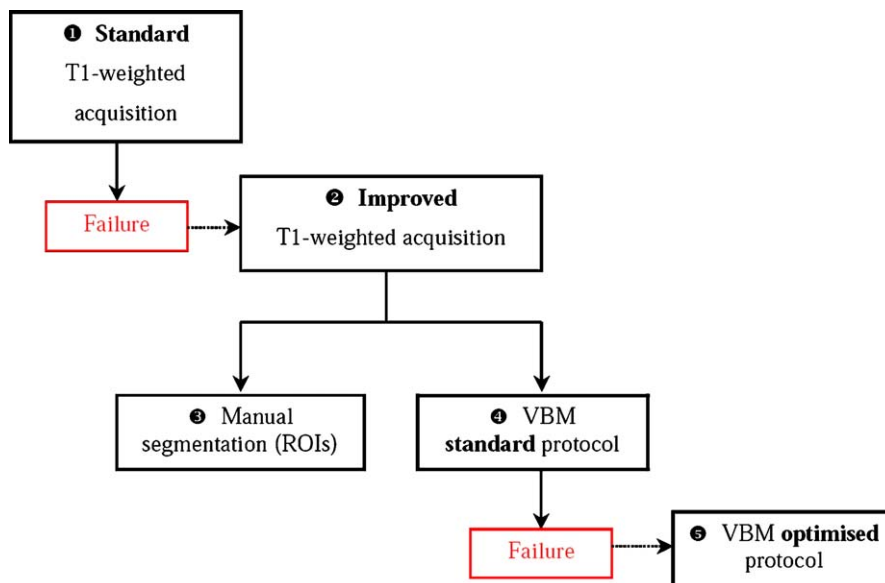


Fig. 1. Schematic diagram of the various steps in image analysis.

delineation was checked in the sagittal and coronal planes. Finally, each ROI was reconstructed in three dimensions to control for the shape of each volume created (Fig. 3). These regions are referred to hereafter as the “subcortical grey nuclei” (SGN).

Voxel-based morphometry (VBM)

1 Standard protocol. VBM is a method implemented within SPM software (Wellcome Department of Cognitive Neurology, London), allowing completely automated voxel-by-voxel statistical analysis of the structural magnetic resonance images obtained from patients and controls. The standard VBM protocol was performed on a Dell workstation Precision 530, using MATLAB 6.1 within the SPM2 version of the SPM software. This protocol is based on several preprocessing steps: a spatial normalisation to align the initial scans in a common stereotactic space (according to the Montreal Neurological Institute [MNI] coordinates), an automated segmentation into grey matter (GM), white matter (WM) and cerebro-spinal fluid (CSF) images and finally, a smoothing by convolving with an isotropic Gaussian kernel, the full-width at half maximum (FWHM) of which is similar to the size of the regional

differences expected between different brains. Thus, the intensity in each voxel of the GM image represents the probability of being a voxel of GM. Here, images were convolved with an 8-mm³ FWHM Gaussian kernel.

However, although the patients in this study had only mild to moderate Huntington’s disease, the spatial transformation did not handle the subcortical atrophy and ventricular enlargement observed in such patients correctly. Indeed, we first tested this normalisation with a non-linear transformation rather than the clearly unsatisfactory affine registration. Nevertheless, the non-linear transformation induced certain artificial deformations (Fig. 4), pulling cortical structures such as the insula or the cingular gyrus towards the inside of the brain. Therefore, we have secondly used a mask to hide the most deformed part of the brain in Huntington’s disease (i.e., the striatum and the lateral ventricles) on the scans of both patients and controls. This mask was applied when estimating the non-linear parameters of the normalisation, so the transformation was based on cortical information only. However, despite these different trials, the subcortical structures of several patients were consistently incorrectly superimposed on the corresponding structures in controls (Fig. 5). This failure of the

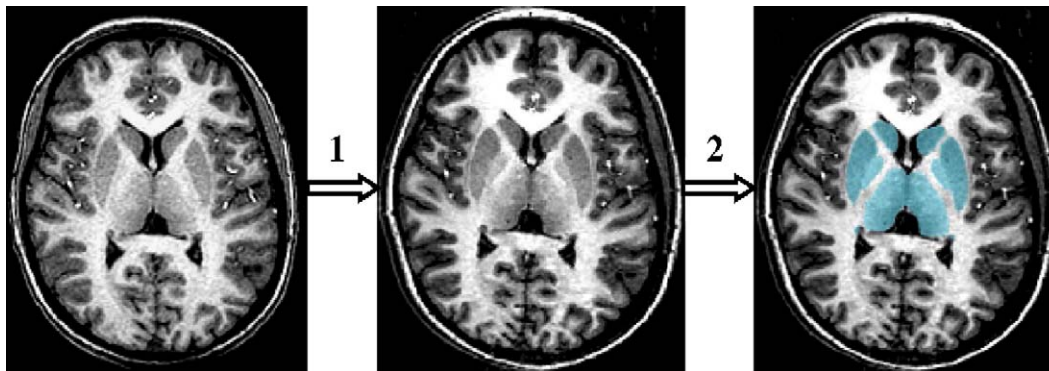


Fig. 2. First step: improvement of the T1-weighted sequence on the MRI of a control (see methods). Second step: superimposition (in blue) of the manual segmentation of the striatum, the globus pallidus and the thalamus on the improved MRI.

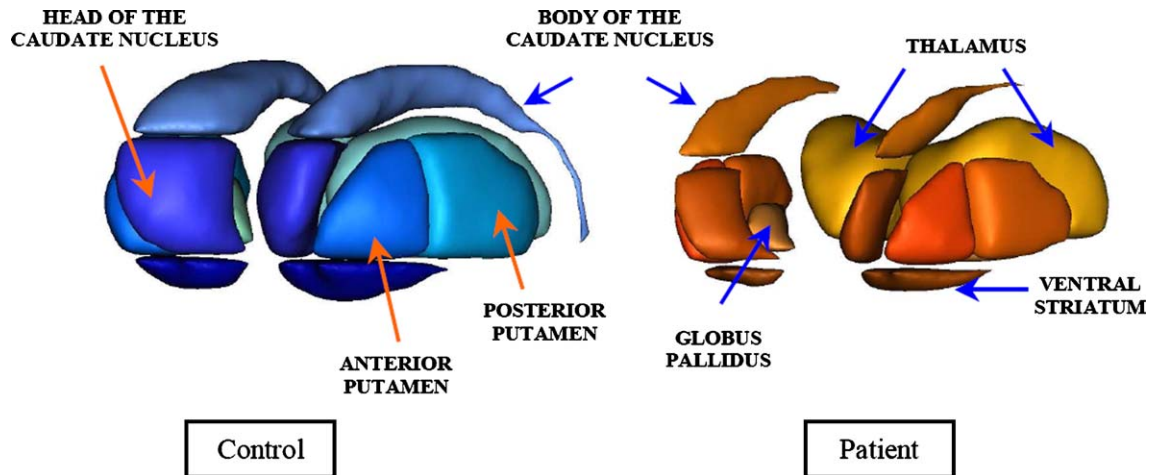


Fig. 3. 3D reconstruction of the various ROIs in the SGN of a control (blue) and a patient (orange) matched for age and sex.

standard VBM protocol justifies our use of an optimised protocol previously described by Good et al. (2001b).

5 Optimised protocol. This optimised VBM protocol involved separate analyses of GM, WM and CSF from the first steps of VBM processing (Good et al., 2001b). We used this protocol to identify relevant information about GM, WM and CSF on our images. In this article, we will focus exclusively on the GM as described in the following.

A template of GM appropriate for this study was created from controls' and patients' images. This made it possible to avoid the bias that would have consisted in favouring one of the two groups in the preprocessing steps. This GM template was obtained by normalising a subset of 12 controls' and 12 patients' scans, together with their respective symmetric images, onto the ICBM 152 template (MNI), by means of an affine transformation. The registered images were then segmented and convolved with a spherical median filter (3 voxels in diameter), which conserves the outlines of the structures and does not introduce new values of

voxel intensity in the voxels. This filtering reduced the number of non-brain and misclassified voxels, most of which were located at the interface between the WM and the lateral ventricles (Fig. 6). A mean image was created from the 24 GM filtered and normalised images and their corresponding 24 symmetric images. Finally, this mean GM image was smoothed with an 8-mm³ Gaussian kernel.

All the preprocessing steps of the optimised VBM protocol were then based on this new template: it was used to have an a priori knowledge of the spatial distribution of GM during the automated segmentation step, and as a GM template for the spatial normalisation of these segmented GM images. Thus, the parameters for non-linear spatial normalisation were estimated from GM information only, whereas in the standard protocol, these parameters are estimated based on 55% GM, 27.5% WM and 17.5% CSF information (Luders et al., 2002). With this preprocessing protocol, the subcortical structures of all patients were correctly superimposed to the same structures in control subjects (Fig. 5).

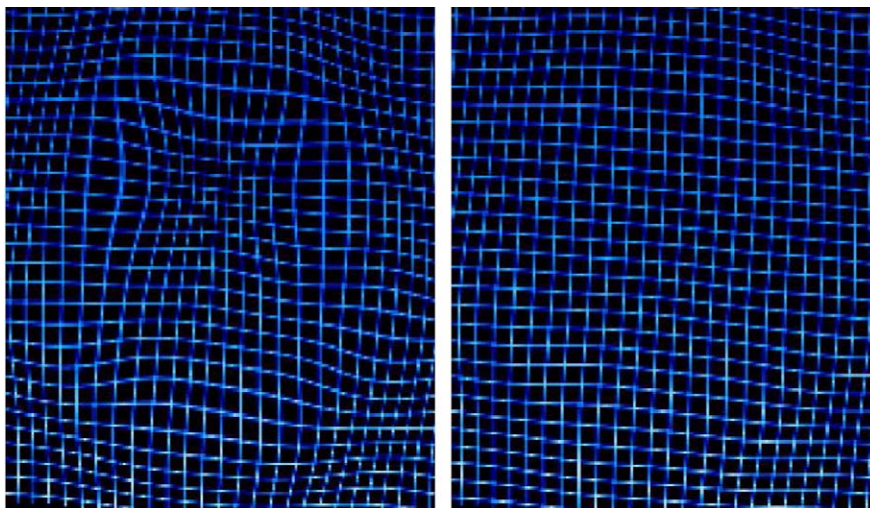


Fig. 4. Results of the application on a grid of a non-linear transformation obtained from the registration of a HD patient scan: (left) without a mask hiding the central parts of the brain; (right) with this mask. Note that, using the mask, the subcortical parts of the brain are not artificially distorted anymore.

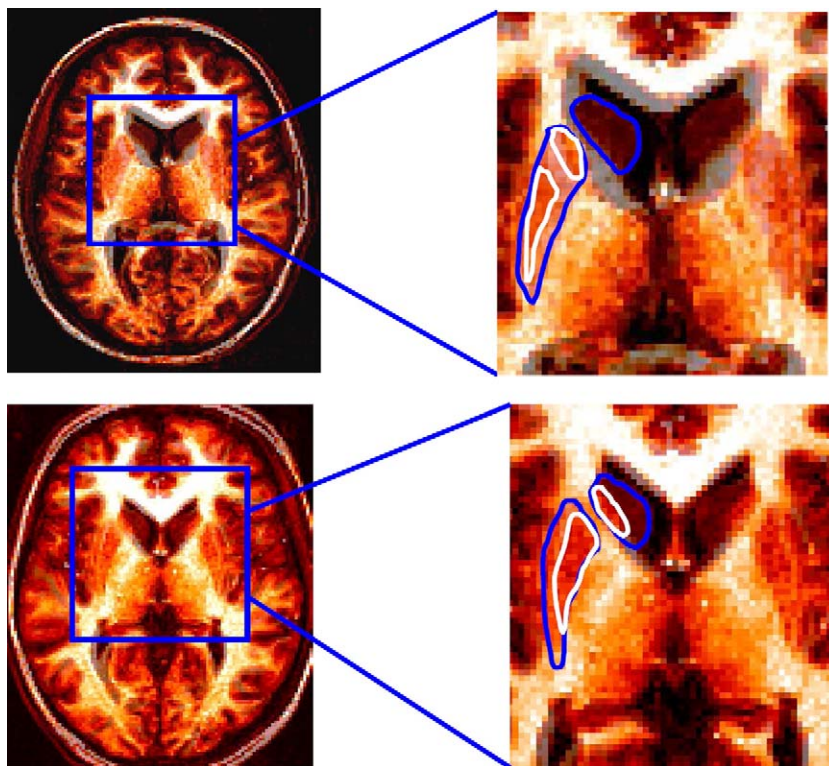


Fig. 5. Up left: merging of the normalised images of a single patient and of a control subject obtained with a non-linear transformation and a mask hiding the central parts of the brain. Up right: zoom on the striatal region showing, in white, the delineation of the head of the caudate and putamen of the patient and, in blue, the same structures for the control. Note that the putamen area of the control includes the head of the caudate of the patient. Down left: the same merged image obtained with the optimised VBM protocol. Down right: zoom on the striatal region. Note that, with the optimised VBM protocol, the putamen area of the control now includes only the putamen of the patient.

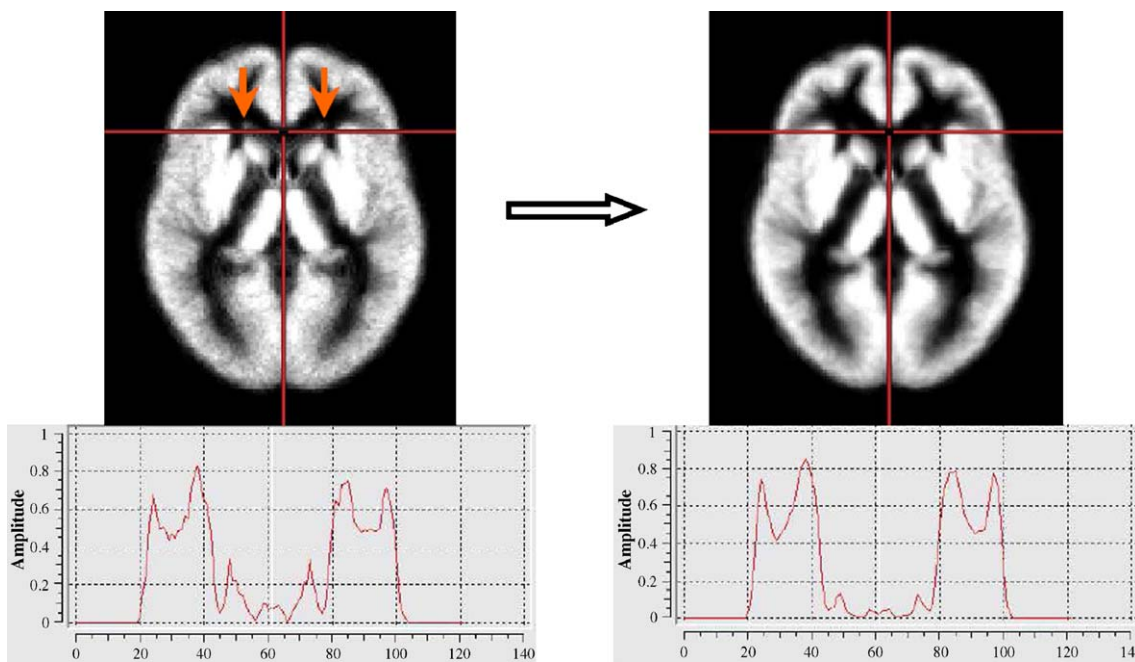


Fig. 6. Up left: the mean GM image (average of the 24 normalised GM images and their respective symmetrics). Up right: the same image convolved with a spherical median filter. Down: histograms of signal intensity in the images. Note that the peaks are located in the same abscissa along x and that the peaks created by the interfaces between frontal horns of lateral ventricles and WM have disappeared.

A “modulation” step was introduced to compensate for the inherent contradiction of VBM (Good et al., 2001b), which detects regional differences in GM between different brains despite inducing non-linear deformations of these brains. Besides, the impact of such non-rigid registration on grey matter data was previously discussed in several publications (Ashburner and Friston, 2001; Bookstein, 2001; Crum et al., 2003). This “modulation” consisted in dividing voxel intensities in the segmented images of GM by Jacobian determinants derived from the spatial normalisation step, these determinants accounting for the non-linear components of this transformation. Modulated normalised GM images were finally smoothed with an 8-mm³ Gaussian kernel.

Concluding strategy

At this stage, the initial MRI acquisition sequence (step 1) and the standard VBM protocol (step 4) were abandoned. Therefore, steps 2, 3 and 5 were adopted for all controls and patients: the manual (step 3) and the automated (step 5) approaches were applied directly to the images supplied by the improved sequence (step 2). All statistical analyses described in the following were performed on data generated from steps 3 and 5.

Statistical inference

Two different analyses were performed on the data obtained by manual segmentation and with the optimised VBM protocol: a group comparison between patients and control subjects and correlation analyses with several clinical scores within the patient group. Though carried out on different data – the volumes of the striatal, pallidal and thalamic regions of each subject on the one hand, and the smoothed, modulated, normalised GM images of these subjects on the other hand – these statistical analyses were made as similar as possible, with the same covariates used in both analyses of covariance (ANCOVA).

Group comparisons

Manual segmentation

The manual segmentation provided the volume (in mm³) of all regions of the SGN in each subject. These volumes, obtained for controls and patients, were compared by ANCOVA using statistical software Datamind (personal communication: Duchesnay et al., 2004). ANCOVA was used to rule out confounding effects engendered by covariates such as age, sex, handedness and education level, which were considered “nuisance” covariates. The choice of these covariates was based on previous VBM studies demonstrating regional anatomical differences when examining the global effects of these covariates in controls (Good et al., 2001a,b; Herve et al., 2005). As the data statistically analysed by VBM were spatially normalised, total intracranial volume (TIV) was also considered as a numerical covariate in order to “normalise” the volumetric data of the SGN. TIV was calculated by summing native GM, WM and CSF volumes. Native GM volume was obtained by dividing the entire volume of the scan by the total intensity of each initial GM image.

Optimised VBM

The smoothed, modulated, normalised GM images were analysed with SPM2, using the framework of a general linear model. Region-specific differences in GM between patients and

controls were assessed by ANCOVA. As mentioned above, age, sex, handedness and education level were included as covariates in the model. For the statistical investigation of differences between both groups, *P* values were corrected for multiple comparisons with the false discovery rate (FDR) — a recent approach controlling for the expected proportion of false positives among suprathreshold voxels. The significance level for this analysis was set at $P < 10^{-2}$ FDR-corrected ($t > 3.98$).

Because a prior hypothesis about regional pathology existed in subcortical grey matter, the same analysis was also limited to ROIs in the SGN, using the Marsbar toolbox included in SPM2 (personal communication: Brett et al., 2002). Marsbar, which calculates the mean of intensity in each region, provides a single *t* value and a single *P* value for each ROI. It therefore quantifies significant atrophy in each structure, complementary to exploration of the statistical *t* map, which provides only the local maximum in each region. These ROIs were defined based on the normalised striatal, pallidal and thalamic regions previously delineated in one control subject.

Correlations

Manual segmentation

We looked for correlations between clinical scores (UHDRS, Purdue Pegboard[®], hand-arm test) and the various SGN volumes within the HD group, considering that TIV might generate a possible confounding effect. All clinical scores were entered in a squared intercorrelation matrix, to exclude from the analyses clinical scores which would be redundant with the others. If clinical tests displayed more than 80% intercorrelation, only one test, arbitrarily selected, was retained. The independence scale score and functional checklist of the UHDRS scores were therefore omitted as they were highly correlated with the TFC. The Stroop C (colour) and W (word) scores were omitted from the analysis as they were correlated with the digit symbol score. These exploratory correlations were considered significant if $P < 0.05$. In addition, we also looked for correlations between the different SGN volumes and CAG repeat length within the HD group.

Optimised VBM

We carried out simple regression analyses with Marsbar to look for correlations between the various clinical scores or CAG repeat numbers and the distribution of GM in each ROI of the SGN in HD patients. TIV was included in the model as a covariate. Results were considered significant at $P < 0.05$.

Results

Improvement of the MRI acquisition sequence

Improvement of the T1-weighted sequence facilitated the manual segmentation because the outlines of several structures, including the posterior putamen, the globus pallidus and the thalamus, appeared more clearly. This sequence improvement also allowed the visualisation of the globus pallidus, which was not visible in all patients with the standard acquisition sequence (Fig. 7). Finally, it came out that this improvement also benefited to the automated segmentation in the optimised VBM protocol, as shown in Fig. 7.

Results in the subcortical grey nuclei (SGN)

Group comparisons

Manual segmentation. The volumes obtained by the manual segmentation in each ROI of the SGN are listed in Table 1, together with the percentage of atrophy found in these structures for the HD patients. The total volume of grey matter and the total intracranial volume were similar to the ones obtained by Luders et al. (2002) in control subjects (Table 1). The mean volumes (averaged over both hemispheres) of these ROIs are also presented in Fig. 8.

An ANOVA revealed that the interaction between groups (patients, control subjects) and ROIs was highly significant (F value=170, P value = 6×10^{-27}), showing that the degree of atrophy was heterogeneous across the various SGN regions. Indeed, the striatal loss of volume exhibited a dorso-ventral gradient, reaching 57% of the mean control value in the dorsal striatum (body of caudate) of HD patients, 51.5% in the medial striatum (head of caudate: 52%, anterior putamen: 53%, posterior putamen: 49%), and 38% in the ventral striatum, while the thalamic loss reached 16% (Table 1). Furthermore, when performing a discriminant analysis with these volumetric data, the ventral striatum was the only region of the striatum that did not correctly classify the 32 subjects in their respective group: 8 were misclassified with the right ventral striatum, and 4 with the left ventral striatum. Finally, GM volume was found significantly lower (–10%) in HD patients than in control subjects (Table 1).

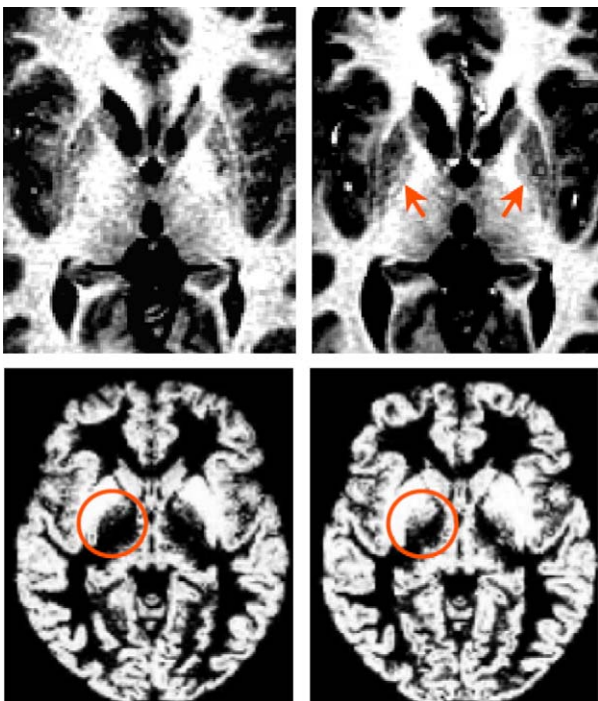


Fig. 7. Up left: striatal region of a patient before improvement of the T1-weighted sequence. Up right: the same region after improvement. Note that the contours of the globus pallidus are now visible (arrows). Down left: normalised grey matter image obtained with SPM2 from a standard acquisition on a control subject. Down right: the same image obtained with the improved MRI sequence. The automated segmentation into grey matter of SPM2 better recognises the globus pallidus as a grey matter structure.

Table 1

Manual segmentation: mean volumes (\pm SD) in mm^3 of the SGN, GM and TIV and percentage of atrophy in HD patients

ROI	Controls		HD patients		Atrophy (%)
	Mean	SD	Mean	SD	
Grey matter	0.79×10^6	16×10^3	0.71×10^6	12×10^3	10
Total intracranial volume	1.58×10^6	34×10^3	1.56×10^6	26×10^3	–
Body of caudate nucleus R	1804	345	727	232	60
Body of caudate nucleus L	1522	334	706	226	54
Head of caudate nucleus R	2167	301	1038	226	52
Head of caudate nucleus L	2349	258	1110	226	53
Anterior putamen R	2345	454	1120	281	52
Posterior putamen R	1746	378	916	138	48
Anterior putamen L	2301	473	1078	250	53
Posterior putamen L	2273	413	1126	217	51
Ventral striatum R	586	141	360	107	39
Ventral striatum L	598	187	376	96	37
Globus pallidus R	1401	222	628	200	55
Globus pallidus L	1449	177	611	162	58
Thalamus R	6421	1054	5455	435	15
Thalamus L	6450	922	5382	428	17

ANCOVA performed on SGN volumetric data proved that all volumes were significantly lower in Huntington's disease patients than in control subjects (Table 2). This analysis revealed that the putamen, the caudate nucleus and the globus pallidus presented the most significant differences between patients and controls whereas the thalamus and the ventral striatum were least affected by the neurodegenerative process.

Optimised VBM. ANCOVA-based voxel-by-voxel comparison of grey matter between the 12 controls and the 20 patients generated a statistical map of t values, which was thresholded at $P < 0.01$ FDR-corrected and overlaid on a normalised patient scan (see Figs. 9a, b). This map revealed highly significant striatal atrophy. The three-dimensional reconstruction of this map merged with the SGN of a control subject demonstrated considerable atrophy in the body of caudate and in the dorsal parts of the head of caudate and putamen, with little damage to the ventral striatum (Fig. 9c). In addition, optimised VBM revealed loss of grey matter in the globus pallidus and in the thalamus.

Besides, the same ANCOVA provided "mean" t value and P value for each ROI of the SGN, using Marsbar (Table 2). The normalised putamen delineated in the normalised GM image of one control subject was also divided into dorsal and ventral putamen. This distinction provided a more precise illustration of the dorso-ventral gradient of striatal atrophy, as a gradient in t values was found in each striatal ROI ($t=9$ for the body of caudate, $t=7.8$ for the head of caudate, $t=7$ for the dorsal putamen, $t=4.4$ for the ventral putamen and finally $t=3.6$ for the ventral striatum, Table 2).

Correlations within the patient group

We assessed possible correlations between the results of clinical tests and the two different measures of SGN grey matter (volume and distribution of GM). We identified 42 correlations significant at the $P < 0.05$ level. In total, 21 of these correlations concerned the same clinical tests and SGN regions with both ROI-based and VBM methods, 4 correlations were seen only with the ROI approach and 17 only with Marsbar (Table 3). The significant correlations revealed in the SGN with Marsbar were also found with a whole-brain voxel-by-voxel approach in VBM. We found no significant correlation between the volumes or the distribution of grey matter in the SGN and CAG repeat numbers.

Results outside the subcortical grey nuclei (SGN)

As optimised VBM needs no prior knowledge on the location of atrophy, it revealed also subcortical loss of grey matter outside the SGN in the substantia nigra (Fig. 10b), the hypothalamus and the amygdala. Optimised VBM additionally evidenced atrophy in several cortical areas, predominantly around the central and the precentral sulci on both hemispheres, and in the left insula (Figs. 10a, c, d). All the local maxima found in the statistical t map provided by VBM outside the SGN are listed in Table 4.

Discussion

This is the first study comparing two different methods for quantifying the atrophy of subcortical grey nuclei associated with Huntington's disease: a manual segmentation and the voxel-based morphometry. These two approaches were previously compared in Alzheimer's disease and schizophrenia but showed some discrepancies in the results concerning the presence or the significance of volume reductions in cortical grey matter (Giuliani et al., 2005; Good et al., 2002; Testa et al., 2004). We show that morphometric measurements in subjects with marked subcortical atrophy are not straightforward and require specific methodological processes. Interestingly, however, when such requirements are met, both automated and manual methods provide comparable results, evidencing a dorso-ventral gradient for striatal atrophy and a significant loss of volume in the globus pallidus and the thalamus. In addition, significant similar correlations are found between several clinical scores rating motor, functional and cognitive disabilities in patients and grey matter measurements

Table 2

Manual segmentation and optimised VBM (Marsbar): ANCOVA results obtained in the SGN, GM and TIV

ROI	Manual Segmentation		Optimised VBM	
	t value	P value	t value	P value
Grey matter	3.38	0.003	NA	NA
Total intracranial volume	0.71	0.49	NA	NA
Body of caudate nucleus R	6.91	$<10^{-5}$	9.32	$<10^{-5}$
Body of caudate nucleus L	6.09	$<10^{-5}$	8.65	$<10^{-5}$
Head of caudate nucleus R	9.36	$<10^{-5}$	7.79	$<10^{-5}$
Head of caudate nucleus L	10.89	$<10^{-5}$	7.77	$<10^{-5}$
Anterior putamen R	8.37	$<10^{-5}$	5.62	$<10^{-5}$
Posterior putamen R	10.28	$<10^{-5}$	5.23	$<10^{-5}$
Dorsal putamen R	NA	NA	6.72	$<10^{-5}$
Ventral putamen R	NA	NA	4.15	2×10^{-4}
Anterior putamen L	8.27	$<10^{-5}$	5.98	$<10^{-5}$
Posterior putamen L	8.48	$<10^{-5}$	5.53	$<10^{-5}$
Dorsal putamen L	NA	NA	7.33	$<10^{-5}$
Ventral putamen L	NA	NA	4.62	5×10^{-5}
Ventral striatum R	2.41	0.02	3.37	0.01
Ventral striatum L	3.75	0.001	3.75	0.004
Globus pallidus R	9.10	$<10^{-5}$	4.92	2×10^{-5}
Globus pallidus L	13.30	$<10^{-5}$	5.10	10^{-5}
Thalamus R	4.97	5×10^{-5}	4.61	5×10^{-5}
Thalamus L	4.89	6×10^{-5}	4.50	6×10^{-5}

for the subcortical grey nuclei. Finally, optimised VBM allows us to detect cortical and subcortical atrophy outside the SGN.

Methodological issues

Improvement of the T_1 -weighted MRI sequence was a crucial first step for the morphometric analyses carried out in this study. Indeed, enhancing the contrast between grey and white matter in the images eased the manual delineation of the various structures. For instance, the outlines of the globus pallidus and the thalamus, which were hardly visible in several previous morphometric studies (Ginovart et al., 1997; Rosas et al., 2003), were readily identifiable here. Moreover, this contrast improvement facilitated the automated recognition of both subcortical and cortical grey matter by VBM.

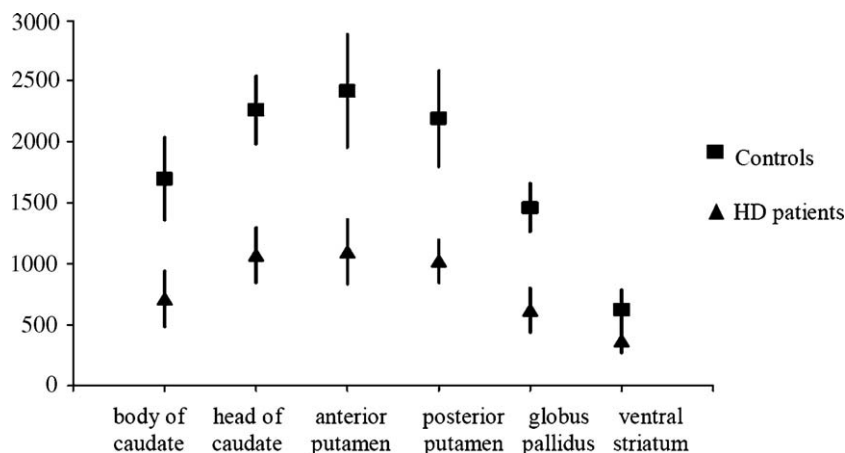


Fig. 8. Manual segmentation: mean (\pm SD) volumes in mm^3 of the striatum and globus pallidus (average L/R).

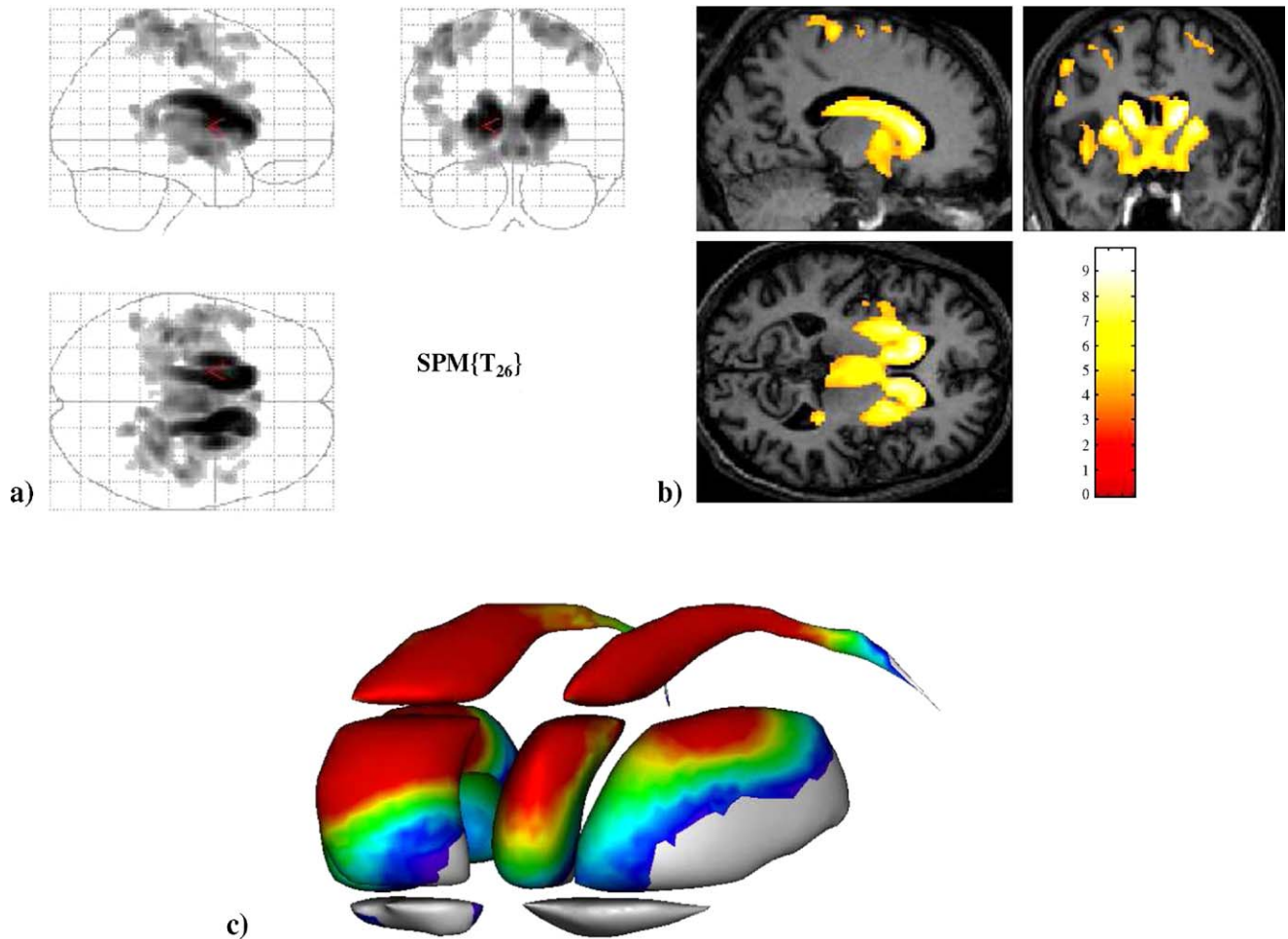


Fig. 9. Optimised VBM: (a) Glassview of the ANCOVA statistical t map thresholded at $P < 0.01$ FDR-corrected. (b) The same t map overlaid on a normalised patient scan. (c) 3D-reconstruction of this t map merged with the striatum of a control subject (grey).

We also showed in this study that use of the optimised VBM (Good et al., 2001b) instead of the standard VBM protocol was a prerequisite for accurate quantification of subcortical atrophy in HD patients. Indeed, the standard protocol did not correctly superimpose the subcortical structures of several patients onto the corresponding structures in the controls. To avoid such caveat, it appeared therefore necessary to analyse the GM, WM and CSF separately, right from the start of VBM processing and to create an appropriate template adapted to this study (Good et al., 2001b).

For the first time, the measurements provided by a manual segmentation were employed to validate the use of the VBM method in Huntington's disease patients. Hence, we reassuringly found comparable results using manual segmentation and optimised VBM for both atrophy measurements and correlation analyses. Indeed, both methods evidenced a specific dorso-ventral gradient in the topography of striatal atrophy and a significant loss of volume in the globus pallidus and the thalamus. Furthermore, correlations between clinical scores and the volumes of the various SGN were found with almost the same motor, functional and cognitive tests, with these two morphometric methods. These results are remarkable given that the two methods are conceptually very different, as manual segmentation supplies individual volumetric data whereas VBM provides statistical differences in the grey matter distribution of smoothed normalised images. Therefore, this exhaustive voxel-wise latter

method, which was first dedicated to analyse cortical structures (Ashburner and Friston, 2000), interestingly proved to correctly manage major subcortical deformations and ventricular enlargements due to marked grey matter loss in the SGN.

However, these two methods differ in terms of cost-benefit analysis. The manual segmentation provides individual data, obtained for each ROI in the native space, without image transformation. Nevertheless, this method is operator-dependent and highly time-consuming. In addition, the subdivision of manually defined regions is subjective and limited, providing restricted knowledge when a continuum of data would be more informative. For instance, we were not able to distinguish the external globus pallidus from the internal globus pallidus or the different thalamic nuclei in our study, and the dorso-ventral gradient of striatal atrophy was only verified at three levels (body of caudate; head of caudate/putamen; ventral striatum). The manual segmentation of some structures such as the body of the caudate nucleus is also subject to great variability (see standard deviations in Table 1). Finally, such a ROI-based approach requires considerable prior knowledge to select the regions that should be analysed and therefore constrains the target of the study.

In contrast, the optimised VBM method answers a statistical question without giving individual volumes. It is, however, completely automated, and therefore unbiased, much less user-

Table 3
Manual segmentation and optimised VBM (Marsbar): correlations

Clinical scores	ROI	Manual segmentation $P < 0.05$	VBM $P < 0.05$
Purdue pegboard®	Head of caudate R	+	+
	Head of caudate L	+	+
	Body of caudate R	+	+
	Body of caudate L	+	+
	Posterior putamen L	+	+
	Ventral striatum L	0	+
	Globus pallidus R	+	0
	Globus pallidus L	+	+
	Thalamus R	0	+
UHDRS Motor	Thalamus L	0	+
	Head of caudate R	+	0
	Head of caudate L	+	0
	Body of caudate R	+	+
	Body of caudate L	+	+
	Posterior putamen L	+	+
	Globus pallidus R	+	0
	Globus pallidus L	+	+
Hand-arm test	Thalamus R	0	+
	Thalamus L	0	+
	Head of caudate R	+	+
	Head of caudate L	+	+
	Body of caudate L	+	+
TFC	Ventral striatum L	0	+
	Globus pallidus L	0	+
	Head of caudate R	+	+
	Head of caudate L	+	+
	Body of caudate R	+	+
	Body of caudate L	+	+
	Posterior putamen L	0	+
	Globus pallidus L	0	+
	Ventral striatum R	0	+
Digit symbol	Thalamus R	0	+
	Thalamus L	0	+
	Head of caudate R	+	+
	Head of caudate L	+	+
	Body of caudate R	+	+
Stroop interference	Body of caudate L	+	+
	Globus pallidus L	0	+
	Body of caudate R	0	+
	Body of caudate L	0	+

dependent and time-consuming than the manual segmentation. VBM also seems to be more sensitive than the ROI approach for demonstration of the dorso-ventral gradient of striatal atrophy or of correlations with clinical scores, although most of the results obtained with the two methods were comparable. Finally, because Huntington's disease induces widespread abnormalities, a method for investigating volume changes in grey matter throughout the brain is required for the correct characterisation of the distribution of neuropathology.

Pathophysiological issues

Both morphometric approaches evidenced the dorso-ventral gradient of striatal atrophy in HD. The optimised VBM revealed

this dorso-ventral gradient even more precisely in the putamen (Fig. 9c, Table 2). This specific topography confirms the results of a previous VBM analysis (Kassubek et al., 2004), and is in line with the results of several histopathological studies in HD patients (review in Vonsattel and DiFiglia, 1998) and in a single asymptomatic subject (Gutekunst et al., 1999). Thus, ventral striatum is the striatal region most spared by the degenerative process. Both approaches proved indeed that the difference of volume between controls and patients was the least significant in ventral striatum (Table 2), in line with previous post mortem studies (Bots and Bruyn, 1981; de la Monte et al., 1988). Accordingly, the reduced degree of atrophy in the ventral striatum (−38%) may explain why the volume of this structure is not sufficient to classify correctly the various subjects of this study in the HD or control group.

Besides, we found a severe atrophy of the globus pallidus, which had lost 56% of the mean normal volume, consistent with the findings of post mortem studies (de la Monte et al., 1988; Halliday et al., 1998; Lange et al., 1976; Mann et al., 1993). Other ROI-based MRI studies (Aylward et al., 1997; Rosas et al., 2003; Fennema-Notestine et al., 2004) also reported a loss of volume in the globus pallidus of HD patients, but this result was not reproduced by previous VBM studies (Kassubek et al., 2004; Thieben et al., 2002). In our study, both ROI-based and VBM methods corroborated the significant pallidal atrophy. This ability to demonstrate the pallidal atrophy may be explained by improvement of the T1-weighted MRI sequence and our use of a median filter.

Moreover, we observed with both methods a moderate atrophy (−16% of the normal volume) in the thalamus confirming histological results (de la Monte et al., 1988; Mann et al., 1993) and previous ROI-based MRI studies (Fennema-Notestine et al., 2004; Ginovart et al., 1997; Jernigan et al., 1991).

The crucial role of basal ganglia degeneration in Huntington's disease is further supported by its implication in the emergence of clinical symptoms, proved by the significant correlations found between several motor scores obtained in our patients and striatal and pallidal atrophy (Table 3). This holds true for performance in cognitive tasks, such as the digit symbol test or the Stroop interference test, which were correlated with the volume of the caudate nucleus (Harris et al., 1996). Finally, we found a highly significant correlation ($P < 0.005$) between the TFC and striatal atrophy. The TFC is a score specifically developed to assess HD progression (Shoulson and Fahn, 1979). It measures the patient's capacity in functional realms and is highly sensitive to early changes in disability (Marder et al., 2000). By showing a strong relationship between TFC score and striatal atrophy, our results further demonstrate the relevance of TFC as a clinical marker of disease progression.

We found no correlation between CAG repeat length and the measures of grey matter in the SGN, apart from a trend between CAG repeats and the volume of the entire striatum ($P < 0.06$). Although such significant correlations were reported in two previous MRI studies (Aylward et al., 1997; Rosas et al., 2001), this result is actually inconsistent and was not reproduced in several post mortem and in vivo studies, both in HD patients and in presymptomatic subjects (Halliday et al., 1998; Harris et al., 1999; Sieradzan et al., 1999; Thieben et al., 2002). This absence of significant correlation in our study might be related to the size of our cohort or to the hypothesis that CAG repeat length is not a main determinant of the atrophy in HD.

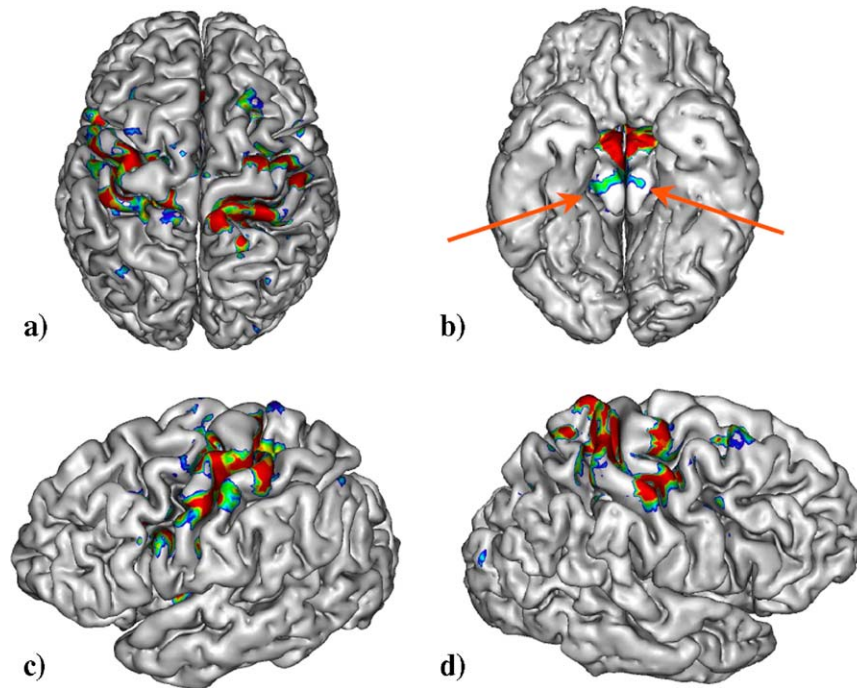


Fig. 10. Optimised VBM: the ANCOVA statistical t map at $P < 0.01$ FDR-corrected merged on the 3D-reconstruction of a normalised control brain. Significant atrophy is observed predominantly around the central and precentral sulci. Note the bilateral atrophy of the substantia nigra (arrows).

Eventually, one major advantage of the VBM approach is that it can detect a regional loss of grey matter without prior knowledge of its location. We therefore found significant atrophy outside the SGN in the substantia nigra, the hypothalamus and the amygdala of the patients included in this study. In the cortex, atrophy was observed in the insular cortex, the precentral and postcentral gyri, and the premotor cortex.

The significant atrophy of the substantia nigra confirms post mortem examinations of HD patients' brains (Deng et al., 2004; Reiner et al., 1988) and one ROI-based study (Fennema-Notestine et al., 2004). It may result from the loss of striatal projections to both the substantia nigra pars compacta and the substantia nigra pars reticulata (Deng et al., 2004). The early loss of striatum-to-substantia nigra pars compacta projection neurones may account

Table 4
Optimised VBM: local peaks outside the SGN obtained with the ANCOVA

Region	L/R	Brodmann area	MNI coordinates (mm)			Talairach coordinates (mm)			Maximal t value
			x	y	z	x	y	z	
Substantia nigra	L	–	–10.5	–21	–10.5	–10.5	–21	–8	4.83
Substantia nigra	R	–	9	–22.5	–12	9	–22.5	–10	4.83
Hypothalamus	L	–	–6	–4.5	–6	–6	–4.5	–5	6.71
Hypothalamus	R	–	4.5	–9	–7.5	4.5	–9	–6	7.31
Amygdala	L	–	–13.5	–1.5	–12	–13.5	–2	–10	5.77
Amygdala	R	–	15.5	–0.5	–12	–15.5	–1	–10	5.46
Central sulcus (sup)	L	4/6	–18	–30	70.5	–18	–26	66	5.85
Central sulcus (sup)	L	4	–40.5	–28.5	69	–40	–24.5	65	7.17
Central sulcus (sup)	R	3/4	30	–34.5	69	30	–30	65	6.83
Central sulcus (sup)	R	4	16.5	–31.5	67.5	16.5	–27.5	63.5	6.60
Central sulcus (mid)	L	3/4	–37.5	–21	49.5	–37	–18	46.5	6.60
Central sulcus (mid)	R	4/6	34.5	–15	49.5	34	–12	46	5.54
Central sulcus (inf)	L	4	–57	–3	30	–56.5	–1.5	27.5	5.39
Precentral sulcus (sup)	L	6	–27	–16.5	70.5	–27	–12.5	65.5	5.84
Precentral sulcus (sup)	R	6	24	–15	70.5	24	–11.5	65.5	6.36
Precentral sulcus (mid)	L	6	–52.5	1.5	49.5	–52	3.5	45.5	5.40
Precentral sulcus (mid)	R	6/9	48	9	46.5	47.5	11	42.5	5.10
Premotor (sup)	R	8	24	12	63	24	14.5	57.5	5.47
Premotor (mid)	L	44	–49.5	18	31.5	–49	19	28	5.71
Insula	L	48	–40.5	–3	–1.5	–40	–3	–1	5.59

for the chorea of HD patients (Hedreen and Folstein, 1995), whereas the loss of projections to the substantia nigra pars reticulata is probably involved in the saccade abnormalities observed in early Huntington's disease (review in Lasker and Zee, 1997; Wurtz and Hikosaka, 1986).

Hypothalamic atrophy in HD patients has been already reported in a few neuropathological and morphometric studies (Kassubek et al., 2004; Kremer et al., 1990, 1991). Although the consequences of hypothalamic degeneration remain unclear, a recent study has demonstrated a low plasma level of testosterone in male Huntington's disease patients, suggesting a loss of hypothalamic dopaminergic neurones (Markianos et al., 2005).

Thus, it is of interest to note that together with the loss of volume in the amygdala that we will discuss in the following, VBM was able to reproduce all subcortical atrophies reported in previous post mortem studies, with the exception of the subthalamic nucleus (STN). This is likely related to the fact that the STN is not detectable in T1-weighted images.

The atrophy of the amygdala demonstrated by VBM was previously reported in two morphometric MRI study (Rosas et al., 2003; Thieben et al., 2002) and in post mortem cases (de la Monte et al., 1988; Mann et al., 1993). This atrophy may result from the disruption of a limbic loop that also involves the ventral striatum, the pallidum and the insular cortex, all regions found to be atrophic in the patients in our study. The degeneration of several relays in this limbic loop may account for some of the emotional and personality disorders observed in patients. For instance, HD patients and gene-positive asymptomatic subjects reveal deficits of recognition of faces exhibiting emotions such as anger, fear and especially disgust (Gray et al., 1997; Sprengelmeyer et al., 1996). Interestingly, damage to the left insula may be associated with a deficit in disgust recognition (Calder et al., 2000), and an fMRI study has shown that presymptomatic subjects have a decreased activation in the left insula when examining facial expressions of disgust (Hennenlotter et al., 2004). At last, as well as in both previous VBM studies that demonstrated an insular atrophy predominating in the left hemisphere (Kassubek et al., 2004; Thieben et al., 2002), we also evidenced significant left insular atrophy in our patients. Altogether, these results suggest that insular atrophy, especially in the left hemisphere, is an early feature of the neurodegenerative process in Huntington's disease and plays a role in the deficits of emotion recognition occurring in subjects carrying the HD mutation.

However, it remains unknown whether the cortical degeneration is a primary or a secondary feature of Huntington's disease degenerative process, or both. The point is that cortical atrophy is now admitted as an earlier and more widespread characteristic of HD than previously expected. In line with this, additionally to insular loss of volume, we found other cortical areas displaying atrophy in the sensorimotor and premotor regions over both hemispheres, in Brodmann's areas 3, 4, 6, 8 and 44 (Table 4). As shown in previous morphometric MRI studies (Kassubek et al., 2004; Rosas et al., 2002), this cortical atrophy predominated in the upper part of the central and precentral regions (Figs. 9a, c, d; Table 4). Interestingly, we observed a significant atrophy in Broca's area in HD patients (Brodmann 44, Table 4), who exhibit motor speech limitations (Murray and Lenz, 2001). Besides, the oculomotor abnormalities observed in Huntington's disease patients (Lasker and Zee, 1997) might be related to the atrophy observed in the frontal eye fields (Brodmann's area 8) together with the one of the substantia nigra pars reticulata, both structures

belonging to the oculomotor loop and being found atrophic thanks to the optimised VBM (Table 4).

Conclusion

This is the first study comparing a manual ROI-based approach and optimised VBM for the quantification of subcortical atrophy in Huntington's disease patients. Although VBM involves spatial deformation to register all the scans into a common space, it happens to correctly handle the principal distortions in the subcortical grey nuclei and ventricles. We thus find that if both techniques provide comparable results, the optimised VBM method presents several advantages. This method is indeed less user-dependent and time-consuming than the manual segmentation. In addition, VBM seems to be more sensitive for revealing the dorso-ventral gradient of striatal atrophy and the correlations between clinical scores and SGN volumes. Finally, VBM requires no prior information concerning the location of the atrophy induced by the neurodegenerative process and has, therefore, revealed grey matter loss outside the SGN examined with our manual morphometric approach. It is remarkable that most of the regions found to be affected by the degenerative process in previous post mortem studies proved also in vivo to be atrophic in VBM whole-brain analysis.

Thus, optimised VBM may represent a sensitive surrogate marker as it provides the most objective quantification of atrophy in carriers of the HD mutation, therefore revealing the extent and progression of the neurodegenerative process. Accordingly, VBM may be used to select patients for clinical trials and to evaluate therapeutic strategies aiming to modify the course of the disease.

Acknowledgments

We thank Jean-François Mangin at the Service Hospitalier Frédéric Joliot for providing helpful advice and comments. This study is part of the MIG-HD program and is supported by the Délégation Régionale à la Recherche Clinique (PHRC AOM0039), the Association Française contre les Myopathies and the Etablissement Français des Greffes.

References

- Ashburner, J., Friston, K.J., 2000. Voxel-based morphometry: the methods. *NeuroImage* 11, 805–821.
- Ashburner, J., Friston, K.J., 2001. Why voxel-based morphometry should be used. *NeuroImage* 14, 1238–1243.
- Aylward, E.H., Li, Q., Stine, O.C., Ranen, N., Sherr, M., Barta, P.E., et al., 1997. Longitudinal change in basal ganglia volume in patients with Huntington's disease. *Neurology* 48, 394–399.
- Bachoud-Lévi, A.-C., Remy, P., Nguyen, J.-P., Brugières, P., Lefaucheur, J.-P., Bourdet, C., et al., 2000. Motor and cognitive improvements in patients with Huntington's disease after neural transplantation. *Lancet* 356, 1975–1979.
- Bloch, J., Bachoud-Levi, A.C., Deglon, N., Lefaucheur, J.P., Winkel, L., Palfi, S., et al., 2004. Neuroprotective gene therapy for Huntington's disease, using polymer-encapsulated cells engineered to secrete human ciliary neurotrophic factor: results of a phase I study. *Hum. Gene Ther.* 15, 968–975.
- Bookstein, F.L., 2001. "Voxel-based morphometry" should not be used with imperfectly registered images. *NeuroImage* 14, 1454–1462.

- Bots, G.T., Bruyn, G.W., 1981. Neuropathological changes of the nucleus accumbens in Huntington's chorea. *Acta Neuropathol. (Berl.)* 55, 21–22.
- Brett, M., Anton, J.L., Valabregue, R., Poline, J.B., 2002. Region of interest analysis using an SPM toolbox. *Proc. 8th HBM, Sendai, Japan* (June).
- Calder, A.J., Keane, J., Manes, F., Antoun, N., Young, A.W., 2000. Impaired recognition and experience of disgust following brain injury. *Nat. Neurosci.* 3, 1077–1078.
- Crum, W.R., Griffin, L.D., Hill, D.L., Hawkes, D.J., 2003. Zen and the art of medical image registration: correspondence, homology, and quality. *NeuroImage* 20, 1425–1437.
- de la Monte, S.M., Vonsattel, J.P., Richardson Jr., E.P., 1988. Morphometric demonstration of atrophic changes in the cerebral cortex, white matter, and neostriatum in Huntington's disease. *J. Neuropathol. Exp. Neurol.* 47, 516–525.
- Deng, Y.P., Albin, R.L., Penney, J.B., Young, A.B., Anderson, K.D., Reiner, A., 2004. Differential loss of striatal projection systems in Huntington's disease: a quantitative immunohistochemical study. *J. Chem. Neuroanat.* 27, 143–164.
- Duchesnay, E., Roche, A., Riviere, R., Papadopoulos-Orfanos, D., Cointepas, Y., Mangin, J.F., 2004. Population classification based on structural morphometry of cortical sulci. *Proc. 2th Proc. IEEE ISBI, Arlington, VA*, pp. 1276–1279 (Apr).
- Fennema-Notestine, C., Archibald, S.L., Jacobson, M.W., Corey-Bloom, J., Paulsen, J.S., Peavy, G.M., et al., 2004. In vivo evidence of cerebellar atrophy and cerebral white matter loss in Huntington disease. *Neurology* 63, 989–995.
- Ginovart, N., Lundin, A., Farde, L., Halldin, C., Backman, L., Swahn, C.G., et al., 1997. PET study of the pre- and post-synaptic dopaminergic markers for the neurodegenerative process in Huntington's disease. *Brain* 120 (Pt. 3), 503–514.
- Giuliani, N.R., Calhoun, V.D., Pearlson, G.D., Francis, A., Buchanan, R.W., 2005. Voxel-based morphometry versus region of interest: a comparison of two methods for analyzing gray matter differences in schizophrenia. *Schizophr. Res.* 74, 135–147.
- Good, C.D., Johnsruide, I., Ashburner, J., Henson, R.N., Friston, K.J., Frackowiak, R.S., 2001a. Cerebral asymmetry and the effects of sex and handedness on brain structure: a voxel-based morphometric analysis of 465 normal adult human brains. *NeuroImage* 14, 685–700.
- Good, C.D., Johnsruide, I.S., Ashburner, J., Henson, R.N., Friston, K.J., Frackowiak, R.S., 2001b. A voxel-based morphometric study of ageing in 465 normal adult human brains. *NeuroImage* 14, 21–36.
- Good, C.D., Scathill, R.I., Fox, N.C., Ashburner, J., Friston, K.J., Chan, D., et al., 2002. Automatic differentiation of anatomical patterns in the human brain: validation with studies of degenerative dementias. *NeuroImage* 17, 29–46.
- Gray, J.M., Young, A.W., Barker, W.A., Curtis, A., Gibson, D., 1997. Impaired recognition of disgust in Huntington's disease gene carriers. *Brain* 120 (Pt. 11), 2029–2038.
- Gutkunst, C.A., Li, S.H., Yi, H., Mulroy, J.S., Kuemmerle, S., Jones, R., et al., 1999. Nuclear and neuropil aggregates in Huntington's disease: relationship to neuropathology. *J. Neurosci.* 19, 2522–2534.
- Halliday, G.M., McRitchie, D.A., Macdonald, V., Double, K.L., Trent, R.J., McCusker, E., 1998. Regional specificity of brain atrophy in Huntington's disease. *Exp. Neurol.* 154, 663–672.
- Harris, G.J., Aylward, E.H., Peyser, C.E., Pearlson, G.D., Brandt, J., Roberts-Twillie, J.V., et al., 1996. Single photon emission computed tomographic blood flow and magnetic resonance volume imaging of basal ganglia in Huntington's disease. *Arch. Neurol.* 53, 316–324.
- Harris, G.J., Codori, A.M., Lewis, R.F., Schmidt, E., Bedi, A., Brandt, J., 1999. Reduced basal ganglia blood flow and volume in pre-symptomatic, gene-tested persons at-risk for Huntington's disease. *Brain* 122 (Pt. 9), 1667–1678.
- Hedreen, J.C., Folstein, S.E., 1995. Early loss of neostriatal striosome neurons in Huntington's disease. *J. Neuropathol. Exp. Neurol.* 54, 105–120.
- Hennenlotter, A., Schroeder, U., Erhard, P., Haslinger, B., Stahl, R., Weindl, A., et al., 2004. Neural correlates associated with impaired disgust processing in pre-symptomatic Huntington's disease. *Brain* 127, 1446–1453.
- Herve, P.Y., Mazoyer, B., Crivello, F., Percey, G., Tzourio-Mazoyer, N., 2005. Finger hand-arm, handedness and grey matter amount in the Rolando's genu area. *NeuroImage* 25, 1133–1145.
- Jernigan, T.L., Salmon, D.P., Butters, N., Hesselink, J.R., 1991. Cerebral structure on MRI: Part II. Specific changes in Alzheimer's and Huntington's diseases. *Biol. Psychiatry* 29, 68–81.
- Kassubek, J., Juengling, F.D., Kioschies, T., Henkel, K., Karitzky, J., Kramer, B., et al., 2004. Topography of cerebral atrophy in early Huntington's disease: a voxel based morphometric MRI study. *J. Neurol., Neurosurg. Psychiatry* 75, 213–220.
- Kremer, H.P., Roos, R.A., Dingjan, G., Marani, E., Bots, G.T., 1990. Atrophy of the hypothalamic lateral tuberal nucleus in Huntington's disease. *J. Neuropathol. Exp. Neurol.* 49, 371–382.
- Kremer, H.P., Roos, R.A., Dingjan, G.M., Bots, G.T., Bruyn, G.W., Hofman, M.A., 1991. The hypothalamic lateral tuberal nucleus and the characteristics of neuronal loss in Huntington's disease. *Neurosci. Lett.* 132, 101–104.
- Lange, H., Thorner, G., Hopf, A., Schroder, K.F., 1976. Morphometric studies of the neuropathological changes in choreatic diseases. *J. Neurol. Sci.* 28, 401–425.
- Langston, J.W., Widner, H., Goetz, C.G., Brooks, D., Fahn, S., Freeman, T., et al., 1992. Core assessment program for intracerebral transplantations (CAPIT). *Mov. Disord.* 7, 2–13.
- Lasker, A.G., Zee, D.S., 1997. Ocular motor abnormalities in Huntington's disease. *Vision Res.* 37, 3639–3645.
- Luders, E., Steinmetz, H., Jancke, L., 2002. Brain size and grey matter volume in the healthy human brain. *NeuroReport* 13, 2371–2374.
- Mann, D.M., Oliver, R., Snowden, J.S., 1993. The topographic distribution of brain atrophy in Huntington's disease and progressive supranuclear palsy. *Acta Neuropathol. (Berl.)* 85, 553–559.
- Marder, K., Zhao, H., Myers, R.H., Cudkovic, M., Kayson, E., Kieburz, K., et al., 2000. Rate of functional decline in Huntington's disease. Huntington Study Group. *Neurology* 54, 452–458.
- Markianos, M., Panas, M., Kalfakis, N., Vassilopoulos, D., 2005. Plasma testosterone in male patients with Huntington's disease: relations to severity of illness and dementia. *Ann. Neurol.* 57, 520–525.
- Morrish, P.K., Sawle, G.V., Brooks, D.J., 1996. Regional changes in [¹⁸F] dopa metabolism in the striatum in Parkinson's disease. *Brain* 119, 2097–2103.
- Murray, L.L., Lenz, L.P., 2001. Productive syntax abilities in Huntington's and Parkinson's diseases. *Brain Cogn.* 46, 213–219.
- Reiner, A., Albin, R.L., Anderson, K.D., D'Amato, C.J., Penney, J.B., Young, A.B., 1988. Differential loss of striatal projection neurons in Huntington disease. *Proc. Natl. Acad. Sci. U. S. A.* 85, 5733–5737.
- Riviere, D., Papadopoulos-Orfanos, D., Poupon, C., Poupon, F., Coulon, O., Poline, J.B., Frouin, V., Regis, J., Mangin, J.F., 2000. A structural browser for human brain mapping. *Proc. 6th HBM: NeuroImage*, 11 (5), p. 912. San Antonio, TX.
- Rosas, H.D., Goodman, J., Chen, Y.I., Jenkins, B.G., Kennedy, D.N., Makris, N., et al., 2001. Striatal volume loss in HD as measured by MRI and the influence of CAG repeat. *Neurology* 57, 1025–1028.
- Rosas, H.D., Liu, A.K., Hersch, S., Glessner, M., Ferrante, R.J., Salat, D.H., et al., 2002. Regional and progressive thinning of the cortical ribbon in Huntington's disease. *Neurology* 58, 695–701.
- Rosas, H.D., Koroshetz, W.J., Chen, Y.I., Skeuse, C., Vangel, M., Cudkovic, M.E., et al., 2003. Evidence for more widespread cerebral pathology in early HD: an MRI-based morphometric analysis. *Neurology* 60, 1615–1620.
- Shoulson, I., Fahn, S., 1979. Huntington disease: clinical care and evaluation. *Neurology* 29, 1–3.
- Sieradzan, K.A., Mehan, A.O., Jones, L., Wanker, E.E., Nukina, N., Mann, D.M., 1999. Huntington's disease intranuclear inclusions contain truncated, ubiquitinated huntingtin protein. *Exp. Neurol.* 156, 92–99.
- Sprenghelmeyer, R., Young, A.W., Calder, A.J., Karnat, A., Lange, H.,

- Homberg, V., et al., 1996. Loss of disgust. Perception of faces and emotions in Huntington's disease. *Brain* 119 (Pt. 5), 1647–1665.
- Steen, R.G., Gronemeyer, S.A., Taylor, J.S., 1995. Age-related changes in proton T1 values of normal human brain. *J. Magn. Reson. Imaging* 5, 43–48.
- Testa, C., Laakso, M.P., Sabattoli, F., Rossi, R., Beltramello, A., Soininen, H., et al., 2004. A comparison between the accuracy of voxel-based morphometry and hippocampal volumetry in Alzheimer's disease. *J. Magn. Reson. Imaging* 19, 274–282.
- Thieben, M.J., Duggins, A.J., Good, C.D., Gomes, L., Mahant, N., Richards, Unified Huntington's Disease Rating Scale, 1996. Reliability and consistency. Huntington Study Group. *Mov. Disord.* 11, 136–142.
- Vonsattel, J.P., DiFiglia, M., 1998. Huntington disease. *J. Neuropathol. Exp. Neurol.* 57, 369–384.
- Vonsattel, J.P., Myers, R.H., Stevens, T.J., Ferrante, R.J., Bird, E.D., Richardson, E.P., 1985. Neuropathological classification of Huntington's disease. *J. Neuropathol. Exp. Neurol.* 44, 559–577.
- Wurtz, R.H., Hikosaka, O., 1986. Role of the basal ganglia in the initiation of saccadic eye movements. *Prog. Brain Res.* 64, 175–190.
- F., et al., 2002. The distribution of structural neuropathology in pre-clinical Huntington's disease. *Brain* 125, 1815–1828.